

Performance Evaluation of Doubly-Fed Induction Generator Using Combined Vector Control and Direct Power Control Method

Khalil Valipour, Reza Najafi*

Electrical and Computer Engineering Department, Mohaghegh Ardabili University,
56517-65835 Germe, Ardabil, Iran

*Corresponding author, e-mail: reza.najafi1369@yahoo.com

Abstract

This paper presents the performance evaluation of Doubly-Fed Induction Generator Using Combined Vector Control and Direct Power Control Method. Combined vector and direct power control (CVDPC) is used for the rotor side converter (RSC) of double-fed induction generators (DFIGs). The control system is according a direct current control by selecting suitable voltage vectors from a switching table. Actually, the proposed CVDPC encompass the benefits of vector control (VC) and direct power control (DPC) in a compact control system. Its benefits compare with VC contains rapid dynamic response, Stability against the machine parameters Changes, less computation, and naive implementation. On the other hand, it has benefits compared with DPC, contains less harmonic distortion and lower power ripple. This technique is to improve the dynamic performance of the DFIG driven by the wind-energy conversion system.

Keywords: doubly-fed induction machine, wind energy conversion systems, CVDPC method.

Copyright © 2016 Institute of Advanced Engineering and Science. All rights reserved.

1. Introduction

Electric energy is one of the most important and highly consumed sources of energy. For a few decades now, the trend of renewable energy for energy generation has been adopted all over the world. The installation of such renewable plants are visible almost everywhere now a days. Due to the global warming issue, change in climate and adoption of green energy concept, most of the countries are deviating from pollution cause sources to environmental friendly sources [1]. Emerging new techniques such as small ignition turbines, fuel cells, wind energy, solar energy and superconducting magnetic energy storage (SMES) make DGs more and more economical and beloved [2]. The purpose has been emerged because the conventional energy sources are finite and have pollution to the environment. About this, wind energy is the most promising renewable energy source among them due to the economically viable [3]. Most of applications of wind power can be found in extensive power range from a few kilowatts to several megawatts in a small scale off grid standalone systems or a large scale grid connected wind farms [4]. Therefore this requires accurate modelling, control and selection of suitable wind energy conversion system.

Vector control is the most popular method used in the DFIG-based WTs [5]. Some of the benefits are precise steady-state performance, lower power ripple, and less converter switching frequency. However, it has some shortcomings, such as its Affiliation on the machine parameters variation due to the decoupling terms and high online computation due to the pulse width modulation (PWM) procedure. Furthermore, the coefficients of proportional–integral (PI) controllers, in the conventional VC, should be optimally tuned to ensure the system stability within the whole operating range and achieve sufficient dynamic response during the transient conditions [6]. This will deteriorate the transient performance of VC and affect the system stability within changing operation conditions. To overcome the aforementioned problems, different nonlinear control procedures such as direct torque control/direct power control (DTC/DPC) have been proposed [7]. The main benefits of DTC/DPC methods contains fast dynamic response, robustness against the machine parameters contains, less computation, and naive implementation. However, they have some shortcomings including significant

torque/power ripples due to the high bandwidth of the hysteresis controllers, variable switching frequency of the converters, and deterioration of the controller performance during the machine starting and low-speed operations. Though many modified methods have been presented to overcome these problems [8], their drawback is complex online computation.

That in this paper is organized as follows: section 1 presents Vector control and direct power control method, section 2 Proposed combined vector control and direct power control, section 4 the control methods of rotor side converter and grid side converter for DFIG, section 5 presented modelling system. The simulation results are shown in section 6, and finally conclusion.

2. Vector Control and Direct Power Control Method

2.1. Vector Control (VC)

The dynamic stator, active and reactive power equations of DFIG in a synchronously (ω_s) rotating d-q reference frame can be expressed by the following Equations [10]:

$$P_s = \frac{3}{2}(V_{ds}I_{ds} + V_{qs}I_{qs}) \quad (1)$$

$$Q_s = \frac{3}{2}(V_{qs}I_{ds} - V_{ds}I_{qs}) \quad (2)$$

The stator voltage vector is aligned with the d axis, therefore V_{qs} is equal to zero and $V_{ds} = V_s$, so the stator active and reactive power equation is simplified to:

$$P_s = \frac{3}{2}V_{ds}I_{ds} \quad (3)$$

$$Q_s = -\frac{3}{2}V_{ds}I_{qs} \quad (4)$$

2.2. Direct Power Control (DPC)

The equations of active and reactive power in DPC method can be expressed as follows [11]:

$$P_s = \frac{3}{2} \frac{L_m}{\sigma L_s L_r} \omega_s |\vec{\lambda}_s| |\vec{\lambda}_r| \sin \delta \quad (5)$$

$$Q_s = \frac{3}{2} \frac{\omega_s}{\sigma L_s} |\vec{\lambda}_s| \left[\frac{L_m}{L_r} |\vec{\lambda}_s| - |\vec{\lambda}_r| \cos \delta \right] \quad (6)$$

$$\delta = \rho_s - \theta_r \quad (7)$$

Where L_s , L_r are the stator and rotor self-inductance, L_m is the mutual-inductance, σ is leakage coefficient, ω_s is the stator angular frequency, δ is the angle between the stator and rotor flux linkage space vector, P_s and θ_r are the angle between σ axis (rotating at electrical angular speed of the rotor ω_m) and their flux linkage as shown in Figure 1. λ_s and λ_r are the stator and rotor flux linkage.

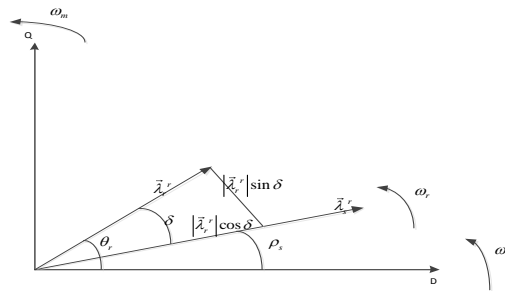


Figure 1. Flux Space Vector in Rotor Reference Frame (OQ)

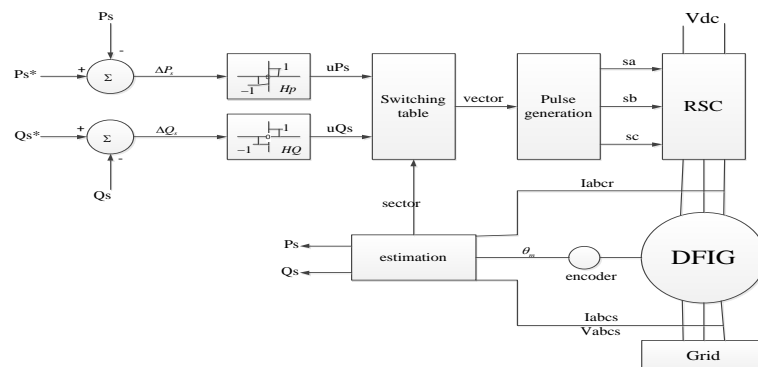


Figure 2. Block Diagram of a DPC for DFIG

The stator windings of DFIG are directly connected to the grid. So under normal conditions, the stator voltage is constant and by neglecting the stator resistance; the stator flux linkage is constant too, so the stator active and reactive power can be written as:

$$P_s = A \left| \vec{\lambda}_r \right| \sin \delta \tag{8}$$

$$Q_s = B \left[C - \left| \vec{\lambda}_r \right| \cos \delta \right] \tag{9}$$

Where A, B and C are constant value. From the above equations, it can be seen stator active power is related to magnitude of rotor flux linkage and sinus of the angle between the stator and rotor flux linkage, as well stator reactive power is related to magnitude of rotor flux linkage and Cosine of the angle between stator and rotor flux linkage, as shown in Figure 1. In direct power control, the stator active and reactive power directly controlled by comparing the reference power with estimated power. The power error is compared with a hysteresis band wide and flags of the hysteresis band wide are specified. The block diagram of this method is shown in Figure 1. Optimal voltage vector can be selected by Knowing rotor flux sector, and the flags of hysteresis comparators. This optimal switching table is shown in Table 1. For example, if the rotor flux linkage vector located in sector I and v2 selected, this voltage vector makes active and reactive power to decrease (the active power will be more negative) and if V3 selected, makes the active power to decrease and reactive power to increase.

3. Proposed Combined Vector Control and Direct Power Control

Due to the vector control, a phase locked loop (PLL) for the stator voltage used, therefore the stator voltage space vector gets along the d axis that rotates at slip speed ($\omega_r = \omega_s - \omega_m$) in the d-q reference frame. So, by neglecting the stator resistance, the stator flux linkage space vector lags the stator voltage space vector by 90 degrees. The location of stator voltage vector and d-q axis in the d-q reference frame is shown in Figure 5 [12].

Table 1. Switching Table for DPC Method

uQ _s	uP _s	sector					
		1	2	3	4	5	6
1	1	V5	V6	V1	V2	V3	V4
	0	V0	V7	V0	V7	V0	V7
	-1	V3	V4	V5	V6	V1	V2
-1	1	V6	V1	V2	V3	V4	V5
	0	V0	V7	V0	V7	V0	V7
	-1	V2	V3	V4	V5	V6	V1

Due to the Equations (8) and (9), the related variations of active power and reactive power are shown by red lines in Figure 3. As shown in this figure, variation of active power is along the d axis, and the variation of reactive power is along the q axis. From equations (3) and (4) and Figure 1, it is concluded:

$$\begin{aligned} \Delta P_s &\propto \Delta I_{ds} \\ \Delta Q_s &\propto -\Delta I_{qs} \end{aligned} \tag{10}$$

It means that the variation of active power is proportional to the variation of d axis stator current and variation of reactive power is proportional to negative variation of q axis stator current. So, d-q axis stator currents can be directly controlled like DPC by a switching table. However, because of the negative relative of reactive power and q axis stator current, the switching table became as Table 2. Figure 4 shows the block diagram of the proposed method which the d -q axis stator currents errors have been compared with a hysteresis band wide. The flags of this comparator and the sector of rotor flux select the voltage vector from Table 2.

4. The Control Methods of Rotor Side Converter and Grid Side Converter for DFIG

Direct power control of voltage source converters has been introduced in [12]. The injected or absorbed Active and reactive power of a voltage source converter directly control by this method. The main idea of this method is like DPC for rotor side converter. However, in GSC instead of rotor flux vector position, the stator voltage vector location defines the sector.

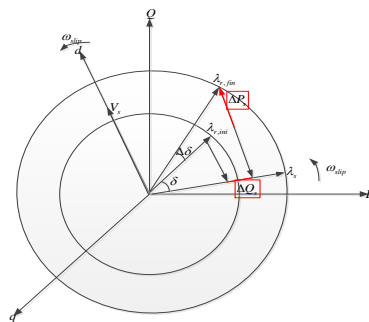


Figure 3. Stator Voltage and Flux in DQ Reference Frame and the Relation of Direct Power to d-q axis Currents

Table 2. Switching Table of Proposed Method for RSC

uQ _s	uP _s	sector					
		1	2	3	4	5	6
1	1	V6	V1	V2	V3	V4	V5
	0	V0	V7	V0	V7	V0	V7
	-1	V2	V3	V4	V5	V6	V1
-1	1	V5	V6	V1	V2	V3	V4
	0	V0	V7	V0	V7	V0	V7
	-1	V3	V4	V5	V6	V1	V2

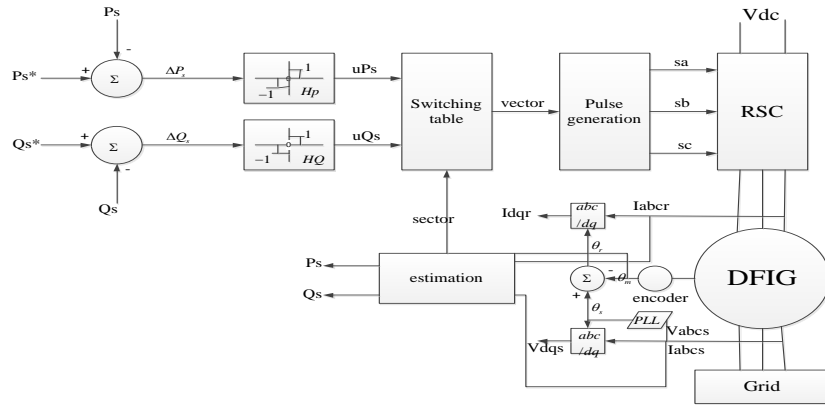


Figure 4. The Block Diagram of Proposed Method for RSC

The voltage of the GSC is the same as voltage of stator windings. By applying phase of the PLL that had been introduced in previous section the grid voltage vector is along the d-axis, thus active and reactive power of the GSC can be simplified as:

$$P_g = \frac{3}{2} V_{dg} I_{dg} \tag{11}$$

$$Q_s = -\frac{3}{2} V_{dg} I_{qg} \tag{12}$$

Variations of GSC active and reactive powers are related to:

$$\begin{aligned} \Delta P_g &\propto \Delta I_{dg} \\ \Delta Q_g &\propto -\Delta I_{qg} \end{aligned} \tag{13}$$

Therefore, the direct current control for GSC can be applied. The block diagram of this method for GSC is displayed in Figure 7. The switching table introduced in [12] changes to Table 3.

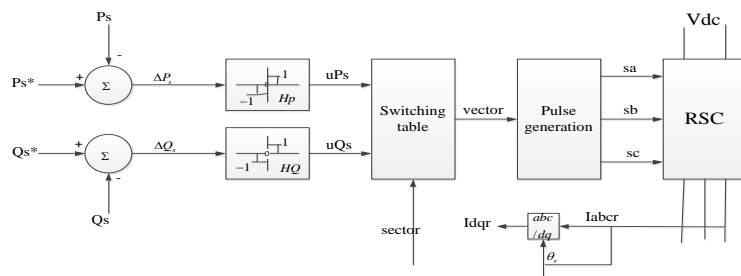


Figure 5. Direct Current Control for GSC

Table 3. Switching Table of Proposed Method for GSC

GSC q axis current	GSC d axis current	sector					
		1	2	3	4	5	6
1	1	V2	V3	V4	V5	V6	V1
	-1	V3	V4	V5	V6	V1	V2
-1	1	V1	V2	V3	V4	V5	V6
	-1	V5	V6	V1	V2	V3	V4

5. Results and Discussion

5.1. Simulation of Turbine Response to a Change in Wind Speed

In this part, the turbine response to a change in wind speed can be seen. At first, wind speed is set at 10 m/s, and then at $t = 0.1$ s, wind speed increases suddenly at 18 m/s. Figure 6 shows the waveforms in relation to the simulation. At $t = 0.1$ s, the generated active power starts increasing gently (together with the turbine speed) to attain its rated value of 2 MW in approximately 0.1s. Over that time frame the turbine speed increases from 1.2 pu to 1.23 pu.

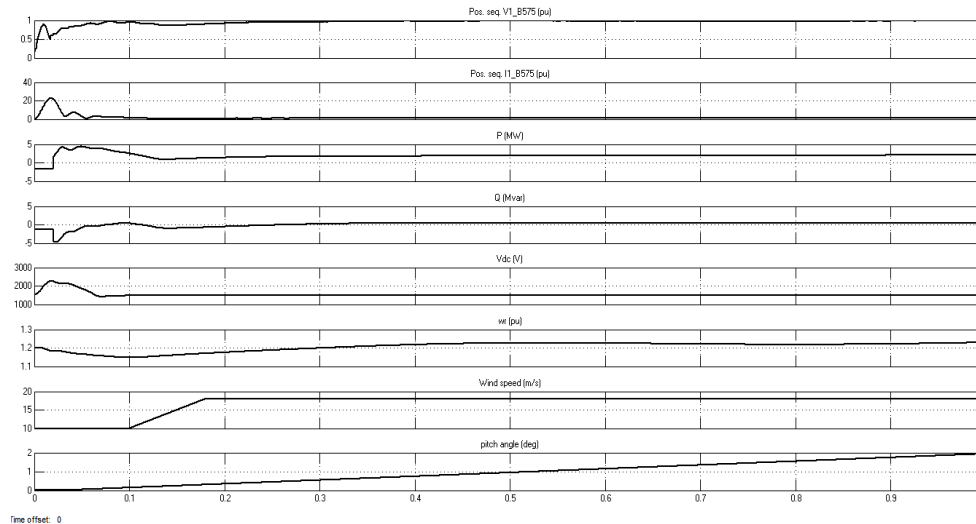


Figure 6. Waveforms for a Gust of Wind in Voltage Regulation Mode

At first, the pitch angle of the turbine blades is zero degree and the turbine operating point follows the red curve of the turbine power characteristics up to point D. Then the pitch angle is increased from 0 deg to 2 deg to limit the mechanical power.

Voltage and the generated reactive power also can be seen. The reactive power is controlled to maintain a 1 pu voltage. At nominal power, the wind turbine absorbs 0.6 MVar (generated $Q=-0.6$ MVar) to control voltage at 1pu. If the mode of operation is changed to Var regulation with the Generated reactive power Q_{ref} set to zero, the voltage increases to 1.02 pu when the wind turbine generates its nominal power at unity power factor.

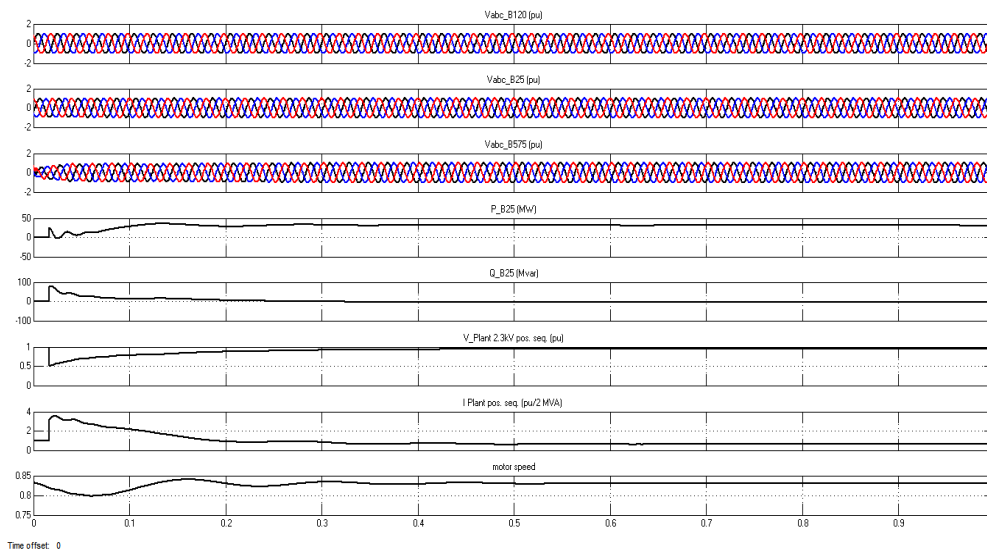


Figure 7. Waveforms for a gust of wind in Var regulation mode

5.2. Simulation of Single Line to Ground Fault on the 25 kV System

In this part, the impact of voltage sag resulting from a remote fault on the 25 kV-system can be seen. In this simulation the mode of operation is initially Var regulation with $Q_{ref}=0$ and the wind speed is constant at 10 m/s. A 0.15 pu voltage drop lasting 0.1 s is programmed, in the B25 voltage source menu, to occur at $t=0.1$ s. The simulation results are illustrated in Figure 8 for voltage regulation mode and Figure 9 for Var regulation mode. The plant voltage and current as well as the motor speed can be seen. Note that the wind farm produces 2 MW. At $t=0.1$ s, the voltage falls below 0.91 pu and at $t=0.2$ s, the protection system trips the plant because an under-voltage lasting more than 0.1 s has been detected (exceeding protection settings for the Plant subsystem). The plant current falls to zero and motor speed decreases gradually, while the wind farm continues generating at a power level of 3 MW. After the plant has tripped, 1.5 MW of power (P_{B25} measured at bus B25) is exported to the grid.

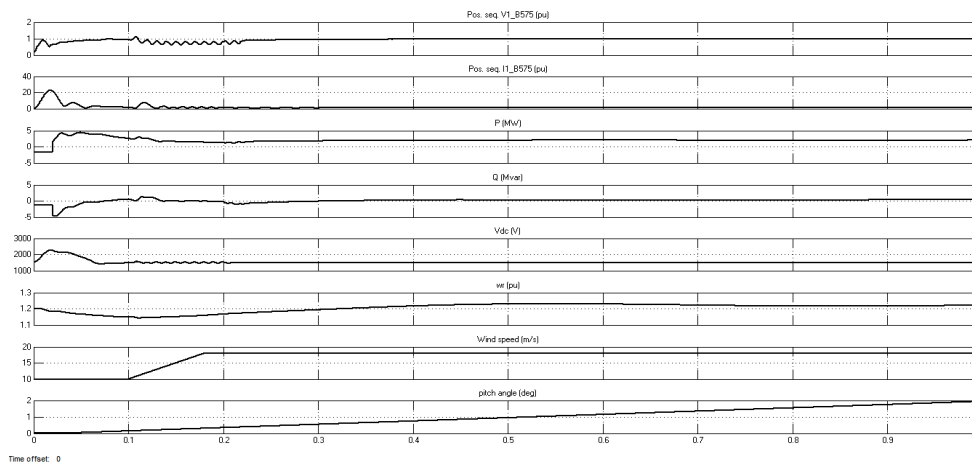


Figure 8. Waveforms for a Single Line to Ground Fault on B25 Bus in Voltage Regulation Mode

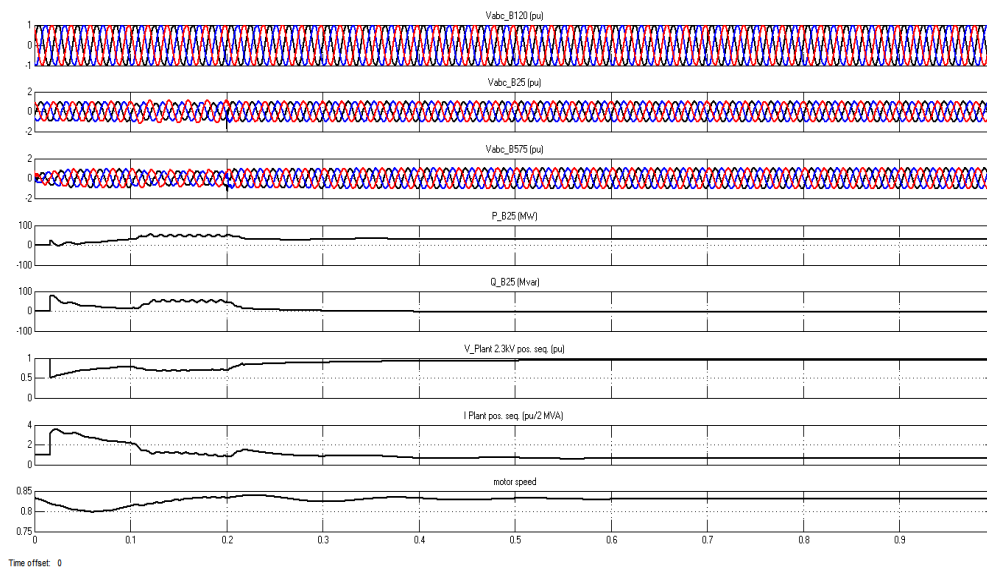


Figure 9. Waveforms for a Single Line to Ground Fault on B25 bus in Var Regulation Mode

As observed in Figure 9 that the plant does not trip anymore. This is because the voltage support provided by the 45 Mvar reactive-power generated by the wind turbines during the voltage sag keeps the plant voltage above the 0.9 pu protection threshold. The plant voltage during the voltage sag is now 0.91 pu.

6. Comparative evaluation

The proposed control system is applied to the Doubly-fed induction machine with parameters as in the Appendix. The wind turbine performance is then simulated, and the results are compared with those obtained by the wind turbine performance under VC and DPC. Figure 10 shows the stator current under the control systems. As can be observed in Figure 11 and 12 the proposed control system contains less harmonic distortion compared to DPC. Compared to DPC Figure 13, 14 and 15 prove that the proposed control system can provide a desirable high performance control of the wind turbine.

Compared to VC in order to evaluate further the control system, a close up of the wind turbine dynamics is presented in Figure 16 by showing the rotor speed, active and reactive power response to a change in wind speed. The figure confirms that the wind turbine response under the proposed control system is compared to VC contains rapid dynamic response and stability against the wind speed changes.

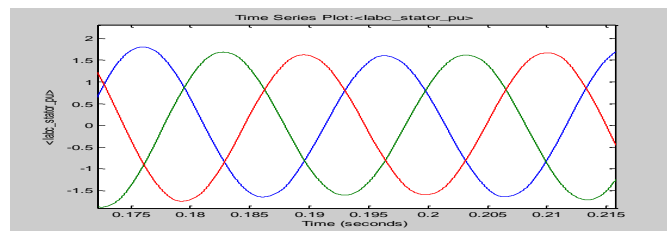


Figure 10. Stator Output Current in Steady-State Conditions

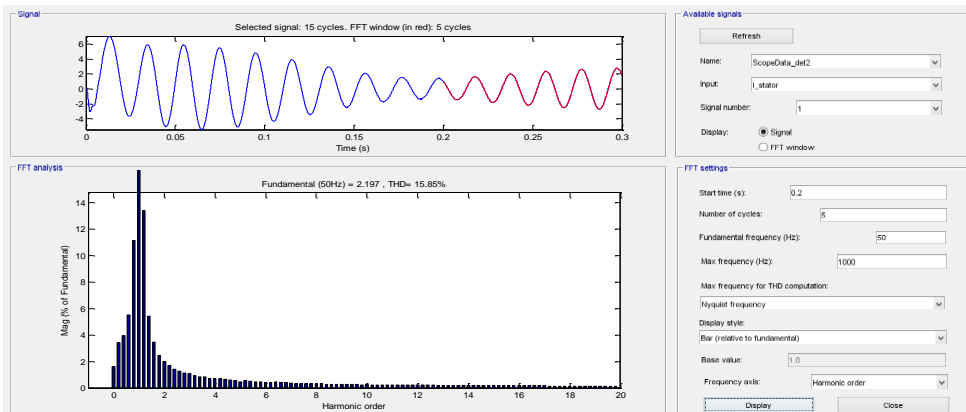


Figure 11. THD of DPC

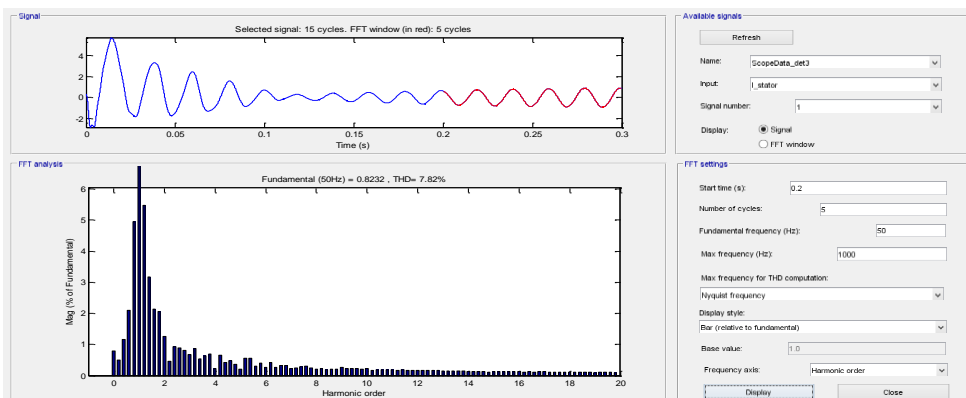


Figure 12. THD of VCDPC

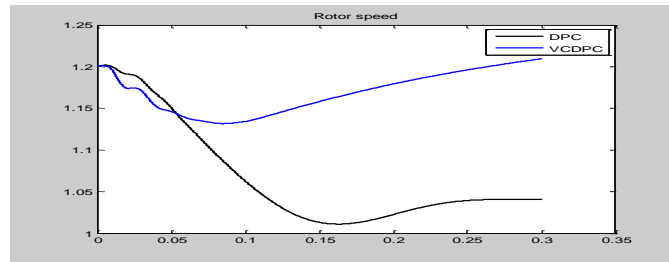


Figure 13. Rotor Speed in Steady-State Conditions

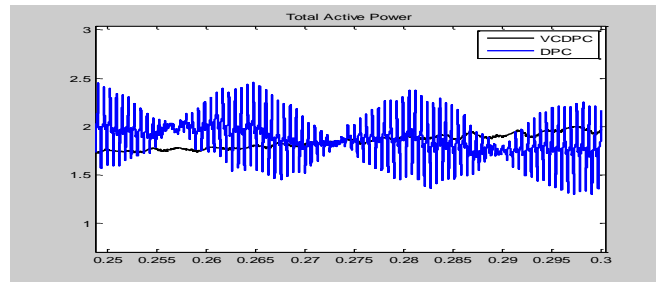


Figure 14. Total Active Power

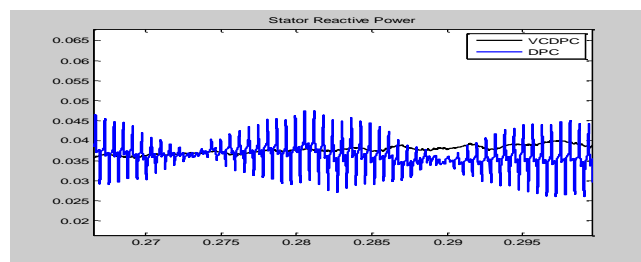


Figure 15. Stator Reactive Power

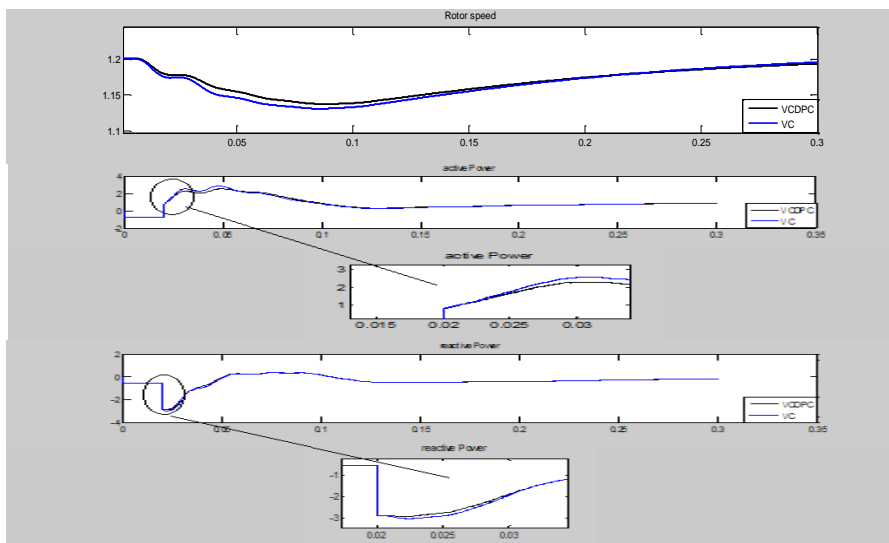


Figure 16. Simulation Results when the Wind Speed Varies

The simulation results presented above confirm that the proposed control system provides wind turbine performances that are better than the results under either DPC or VC.

7. Conclusion

This paper presents the performance evaluation of Doubly-Fed Induction Generator Using Combined Vector Control and Direct Power Control Method. Combined vector and direct power control is used for the rotor side converter of double-fed induction generators. The results of a single line to ground fault and a symmetrical three-phase ground fault is analysed. The results show that the wind energy conversion system can normally operate in fault conditions.

References

- [1] K Viswanadha, S Murthy, M Kirankumar, GRK Murthy. A Performance Comparison of DFIG using Power Transfer Matrix and Direct Power Control Techniques. *International Journal of Power Electronics and Drive System (IJPEDS)*. 2014; 5(2): 176-184.
- [2] A Jamal, S Suropto, R Syahputra. Performance Evaluation of Wind Turbine with Doubly-Fed Induction Generator. *International Journal of Applied Engineering Research*. 2016; 11(7): 4999-5004.
- [3] JS Sathiyarayanan, A Senthilkumar, J Jayashree. Performance Evaluation of Doubly Fed Induction Generator Using Neural Network. *World Applied Sciences Journal*. 2016; 33(5): 769-776.
- [4] R Syahputra. Fuzzy Multi-Objective Approach for the Improvement of Distribution Network Efficiency by Considering DG. *International Journal of Computer Science & Information Technology (IJCSIT)*. 2012; 4(2): 57-68.
- [5] S Li, TA Haskew, KA Williams, RP Swatloski. Control of DFIG wind turbine with direct-current vector control configuration. *IEEE Trans. Sustain. Energy*. 2012; 3(1): 1-11.
- [6] L Xu, P Cartwright. Direct active and reactive power control of DFIG for wind energy generation. *IEEE Trans. Energy Convers.* 2006; 21(3): 750-758.
- [7] J Hu, H Nian, B Hu, Y He. Direct active and reactive power regulation of DFIG using sliding-mode control approach. *IEEE Trans. Energy Convers.* 2010; 25(4): 1028-1039.
- [8] AJ Sguarezi Filho, ER Filho. Model-based predictive control applied to the doubly-fed induction generator direct power control. *IEEE Trans. Sustain. Energy*. 2012; 3(3): 398-406.
- [9] A Jamal, S Suropto, R Syahputra. Performance Evaluation of Wind Turbine with Doubly-Fed Induction Generator. *International Journal of Applied Engineering Research*. 2016; 11(7): 4999-5004.
- [10] R Pena, JC Clare, GM Asher. Doubly fed induction generator using back-to-back PWM converters and its application to variable-speed wind-energy generation. *Inst. Electr. Eng. Proc. Elect. Power Appl.* 1996; 143(3): 231-241.
- [11] J Mohammadi, S Vaez-Zadeh, S Afsharnia, E Daryabeigi. A Combined Vector and Direct Power Control for DFIG-Based Wind Turbines. *IEEE Trans. Sustainable Energy*. 2015; 5(3): 760-775.
- [12] ME Zarei, B Asaei. *Combined Vector Control and Direct Power Control Methods for DFIG under Normal and Unbalanced and Distorted Grid Voltage Conditions*. 4th Power Electronics, Drive Systems & Technologies Conference (PEDSTC2013). Tehran, Iran. 2013.